Semiconductor Physics, Quantum Electronics & Optoelectronics, 2014. V. 17, N 2. P. 149-154.

PACS 78.20.Fm, 87.10.Rt, 87.15.ak, 87.16.af

Modeling of light scattering in biotissue

P.V. Ivashko
Chernivtsi National University,
2, Kotsyubinsky str., 58012 Chernivtsi, Ukraine
E-mail: paul.ivashko@gmail.com

Abstract. Different statistical modeling techniques of radiation propagation in epithelial tissue are considered. The two main approaches are: the modified classical Monte Carlo method for light propagation in turbid medium and the coherent inverse ray tracing method. The classical Monte Carlo method was modified to take into account polarization of propagating radiation and birefringence, which can occur due to tissues commonly found under epithelium. As a supplementary method, used in the paper was a modified version of the classical ray tracing technique, which takes into account phase of radiation during its propagation in tissue.

Keywords: Monte Carlo method, simulation, biological tissue, epithelial tissue, polarization, birefringence.

Manuscript received 31.01.14; revised version received 24.04.14; accepted for publication 12.06.14; published online 30.06.14.

1. Introduction

One of approaches for solving the problem of light propagation in scattering media is the method of Monte Carlo statistical simulation [1-5]. It is a set of techniques that enables to find necessary solutions by repetitive random sampling. Estimates of the unknown quantities are performed with statistical means.

For the case of radiation transfer in scattering medium, the Monte Carlo method implies repeated calculations of the photon trajectory in medium based on determining environmental parameters. Application of the Monte Carlo method is based on the use of macroscopic optical properties of the medium that is considered to be homogeneous within small volumes of tissue. The models based on this method can be divided into two types: the models that take into account polarization of radiation, and the ones that ignore it.

Simulation based on the previous models usually discards the details of the radiation energy distribution within a single scattering particle. This disadvantage can be ruled out (in the case of scattering particles' size exceeding the wavelength) by using another method – reverse ray tracing. This method, similar to that mentioned above, is based on passing a large number of photons through medium that is simulated. The difference is that each scattering particle has a certain geometric topology, and scattering is calculated using the Fresnel equations. The disadvantage of this method is that it can give reliable results only if the particle size is much greater than the wavelength (at least by an order of magnitude).

2. Simulation of polarized radiation propagation in scattering medium by using the Monte Carlo method

The Monte Carlo method is used for implementing the stochastic model, in which the expected value of the random variable is equivalent to the value of the physical quantity that must be determined. This expected value is determined by averaging many independent samples of the random variable. To build a series of independent samples, random numbers are taken from the probability distribution corresponding to the distribution of the physical quantity.

Radiation is represented by a set of photons. Each photon propagating inside medium has a certain amount of energy, position, direction and polarization [6-9]. When modeling propagation of photons in environment,

the following assumption is made: events of radiation scattering by the particles are independent; distributed environment, in which radiation appears, is one-axis material with linear birefringence; dispersion in this environment occurs on spherical particles that are randomly distributed inside it.

During simulation, two coordinate systems are used: the laboratory coordinate system that is bound to the environment of propagation and the local coordinate system that is bound to photon and changes after each scattering event.

The geometry of the model is shown in Fig. 1.

Radiation in the form of a thin beam penetrates into the medium towards the positive direction of the *Z* axis (laboratory coordinate system). The slow linear birefringence axis is directed along the axis *X*. In the environment, photons are scattered by spherical particles. This scattering is described by the Mie theory. The detector is located in the *XY* plane of the laboratory coordinate system and shown in the figure in grey color. It captures only photons coming out from the environment.

The whole algorithm is shown in Fig. 2.

The first step in modeling is to launch one of several million photons in the medium. The reference plane of polarization is chosen (vectors **u** and **v** of the local coordinate system), and the Stokes vector describing the polarization state of the incident beam is selected [1].

Two single vectors are used to set the reference plane: **v** = [0, 1, 0] and **u** = [0, 0, 1]. Vector **u** indicates the initial direction of propagation of photon. For any type of polarization, the incident beam is given by the Stokes vector **S** = [IQUV], which plane of reference was defined above.

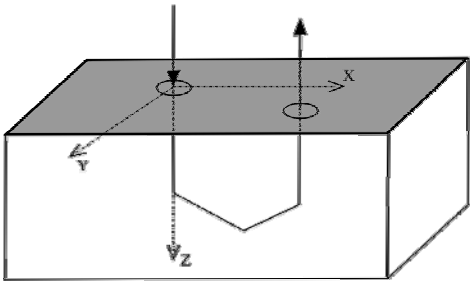

Fig. 1. Geometry of the model.

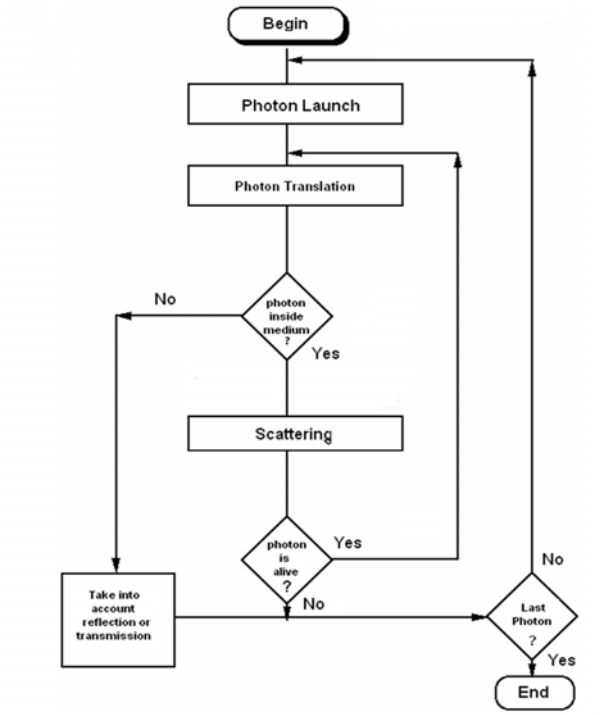

Fig. 2. Block diagram of the algorithm.

Photon moves a distance ΔS that is calculated on the basis of the random number ζ that lies within the range (0, 1].

$$\Delta S = -\frac{\ln(\zeta)}{\mu_t}. \qquad (1)$$

Here, $\mu_t = \mu_a + \mu_s$ is the interaction coefficient, μ_a – absorption coefficient, μ_s – scattering coefficient.

The photon trajectory is characterized by directing cosines $[u_x, u_y, u_z]$. The photon position is changed from $[x', y', z']$ to $[x, y, z]$ as follows:

$$\begin{aligned} x' &= x + u_x \Delta S, \\ y' &= y + u_y \Delta S, . \\ z' &= z + u_z \Delta S. \end{aligned} \qquad (2)$$

The birefringence effect is taken into account by using a linear delay represented by the matrix:

$$T(\Delta, \beta) = \begin{bmatrix} 1 & 0 & 0 & 0 \\ 0 & C_4 \sin^2\left(\frac{\Delta}{2}\right) + \cos^2\left(\frac{\Delta}{2}\right) & S_4 \sin^2\left(\frac{\Delta}{2}\right) & -S_2 \sin(\Delta) \\ 0 & S_4 \sin^2\left(\frac{\Delta}{2}\right) & -C_4 \sin^2\left(\frac{\Delta}{2}\right) + \cos^2\left(\frac{\Delta}{2}\right) & C_2 \sin(\Delta) \\ 0 & S_2 \sin(\Delta) & -C_2 \sin(\Delta) & \cos(\Delta) \end{bmatrix}, \qquad (3)$$

$C_2 = \cos(2\beta)$, $S_2 = \sin(2\beta)$, $S_4 = \sin(4\beta)$,

where β is the azimuthal angle of the slow axis of birefringence in the *XY* plane local coordinate system of photon, Δ – delay that can be obtained as follows:

$$\Delta = \Delta n \frac{2\pi S}{\lambda'}. \quad (4)$$

Here Δn is the difference between the maximum and minimum refractive indexes in the plane perpendicular to the direction of photon, S – path that went photon (react of scattering), λ' – length of light wave in the medium sample.

If you know the angle between the slow axis of birefringence and direction of motion of photon, it can be calculated by the formula:

$$\Delta n = \frac{n_s n_f}{\sqrt{(n_s \cos\alpha)^2 + (n_f \sin\alpha)^2}} - n_f, \quad (5)$$

where n_s and n_f are the refractive indexes along the slow and fast axes of birefringence, which satisfy the relation:

$$n_s = n_f + \delta, \quad (6)$$

where δ is the value of linear birefringence.

The Stokes vector is multiplied by matrix before each act of scattering. Absorption of radiation in the environment is caused by the weight of photon *W*, which is adjusted after each event of absorption in accordance with the albedo of the medium.

$$\text{albedo} = \frac{\mu_s}{\mu_s + \mu_a}. \quad (7)$$

Albedo is partial probability of photon scattering. The initial weight of photon is equal to 1. After the *n*-th event of absorption, the weight is equal to $(\text{albedo})^n$. When the photon weight decreases to critical levels, it is completely absorbed. If photon comes from with a certain weight *W*, the corresponding Stokes vector is multiplied by *W* to account for photon attenuation.

$$\begin{vmatrix} I \\ Q \\ U \\ B \end{vmatrix} = \begin{vmatrix} I \cdot W \\ Q \cdot W \\ U \cdot W \\ B \cdot W \end{vmatrix}. \quad (8)$$

Step 2. One of the most important steps in the process of modeling is choosing the angles α (scattering angle) and β (angle in the plane of scattering) (Fig. 3).

Choosing these angles is based on the phase function. For polarized radiation $S_0 = [I_0, Q_0, U_0, V_0]$, it looks like:

$$\theta(\alpha,\beta) = m_1(\alpha) I_0 + m_2(\alpha) Q_0 \cos(2\beta) + m_2(\alpha) U_0 \sin(2\beta). \quad (9)$$

Where $m_1(\alpha)$ and $m_2(\alpha)$ are the elements of the scattering matrix:

$$M(\alpha) = \begin{bmatrix} m_1(\alpha) & m_2(\alpha) & 0 & 0 \\ m_2(\alpha) & m_1(\alpha) & 0 & 0 \\ 0 & 0 & m_3(\alpha) & m_4(\alpha) \\ 0 & 0 & -m_4(\alpha) & m_3(\alpha) \end{bmatrix}. \quad (10)$$

The matrix determines the polarization properties of the scattering element. In the case of spherical scattering, the particles scattering matrix is symmetrical. The elements $m_1(\alpha)$, $m_2(\alpha)$, $m_3(\alpha)$ and $m_4(\alpha)$ are related to the scattering amplitudes:

$$m_1(\alpha) = \frac{1}{2}\left(|S_2|^2 + |S_1|^2\right),$$
$$m_2(\alpha) = \frac{1}{2}\left(|S_2|^2 - |S_1|^2\right),$$
$$m_3(\alpha) = \frac{1}{2}\left(S_2^* S_1 + S_2 S_1^*\right),$$
$$m_4(\alpha) = \frac{1}{2}\left(S_1 S_2^* - S_2 S_1^*\right). \quad (11)$$

We introduce some notations:

• particle size $x = kr$, where r – radius of the sphere, $k = \frac{2\pi}{\lambda}$;

• complex index of refraction $m = \nu - k$;

$$S_1(m,x,\theta) = \sum_{n=1}^{\infty} \frac{2n+1}{n(n+1)}\left(a_n \pi_n + b_n \tau_n\right),$$
$$S_2(m,x,\theta) = \sum_{n=1}^{\infty} \frac{2n+1}{n(n+1)}\left(b_n \pi_n + a_n \tau_n\right). \quad (12)$$

Coefficients π_n and τ_n are functions of $\mu = \cos\theta$:

$$\pi_n(\theta) = \cos\theta \frac{2n-1}{n-1}\pi_{n-1}(\theta) - \frac{1}{n-1}\pi_{n-2}(\theta),$$
$$\tau_n(\theta) = \cos\theta\left[\pi_n(\theta) - \pi_{n-2}(\theta)\right] -$$
$$-(2n-1)\sin^2\theta\,\pi_{n-1}(\theta) + \tau_{n-2}(\theta),$$
$$0 \le \theta \le \pi, \quad (13)$$

where

$$\pi_0(\theta) = 0, \quad \tau_0(\theta) = 0,$$
$$\pi_1(\theta) = 1, \quad \tau_1(\theta) = \cos\theta,$$
$$\pi_2(\theta) = 3\cos\theta, \quad \tau_2(\theta) = 3\cos 2\theta. \quad (14)$$

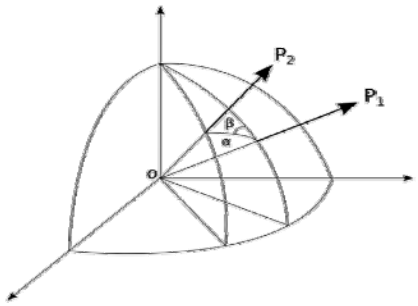

Fig. 3. Directions of photon scattering before and after interaction.

In the cases of $\theta = 0$ and $\theta = \pi$, these coefficients are reduced to the following form:

$$\pi_n(0) = \tau_n(0) = \frac{n(n+1)}{2},$$
$$-\pi_n(\pi) = \tau_n(\pi) = (-1)^n \frac{n(n+1)}{2}. \quad (15)$$

Coefficients a_n and b_n are functions of m and x:

$$a_n(m,x) = \frac{\left(\frac{A_n(y)}{m} + \frac{n}{x}\right)\mathrm{Re}\{w_n(x)\} - \mathrm{Re}\{w_{n-1}(x)\}}{\left(\frac{A_n(y)}{m} + \frac{n}{x}\right)w_n(x) - w_{n-1}(x)},$$
$$b_n(m,x) = \frac{\left(mA_n(y) + \frac{n}{x}\right)\mathrm{Re}\{w_n(x)\} - \mathrm{Re}\{w_{n-1}(x)\}}{\left(mA_n(y) + \frac{n}{x}\right)w_n(x) - w_{n-1}(x)}, \quad (16)$$

where

$$w_x(x) = \frac{2n-1}{x}w_{n-1}(x) - w_{n-2}(x),$$
$$w_0(x) = \sin(x) - i\cos(x),$$
$$w_{-1}(x) = \cos(x) - i\sin(x). \quad (17)$$

The expression for $A_n(y)$ looks like:

$$A_n(y) = -\frac{n}{y} + \left[\frac{n}{y} - A_{n-1}(y)\right]^{-1},$$
$$A_0(y) = \frac{\sin(p)\cos(p) + i\sinh(q)\cosh(q)}{\sin^2(p) + \sinh^2(q)}. \quad (18)$$

The summation in expression (8) is reduced to $n \approx x$.

Step 3. We calculate the Stokes vector for the back scattering at the angle ψ to its reference plane coinciding with the plane of scattering. This is achieved by rotating the matrix

$$R(\beta) = \begin{bmatrix} 1 & 0 & 0 & 0 \\ 0 & \cos(2\beta) & \sin(\beta 2) & 0 \\ 0 & -\sin(\beta 2) & \cos(2\beta) & 0 \\ 0 & 0 & 0 & 1 \end{bmatrix}. \quad (19)$$

Correction of the Stokes vector is as follows:

$$S = M(\alpha)R(\beta)S. \quad (20)$$

3. Simulation results for different values of birefringence

In simulation (Figs 4-6), the following system parameters [10-14] were used: the refractive index of the scattering particle – 1.57, the refractive index of the medium around the particles – 1.33, the diameter of the scattering particles – 0.35 μm, the wavelength equal to 0.6328, absorption coefficient – 1 cm^3, scattering coefficient – 90 cm^3, the thickness of the material along the *Z*-axis – 0.2 cm, the number of photons – 1000000.

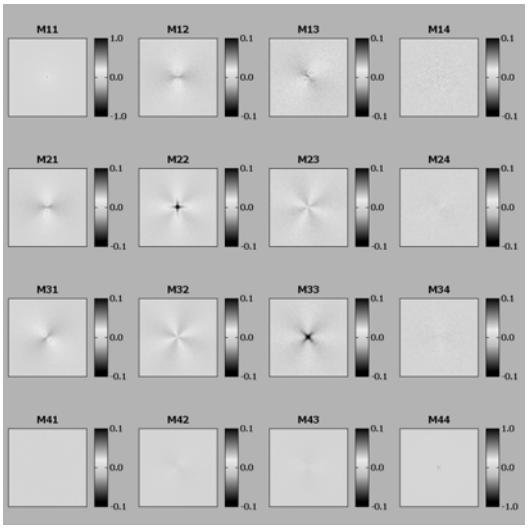

Fig. 4. The slow axis of birefringence of 1.331, fast axis 1.33.

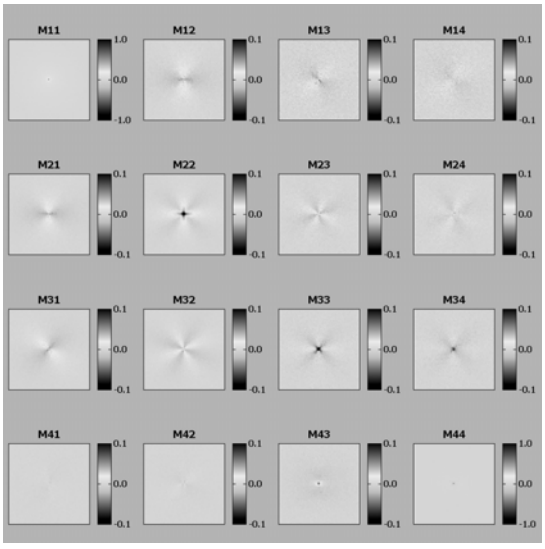

Fig. 5. The slow axis of birefringence 10,331, fast axis 1.33.

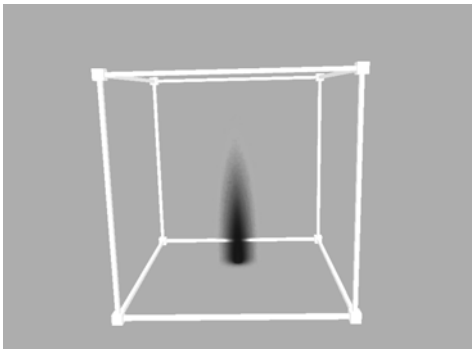

Fig. 6. Distribution of the intensity of absorbed radiation in the environment.

4. Simulation of coherent radiation propagation by using the reverse ray tracing method

The reverse ray tracing method is based on modeling the passage of light beams (photon packets) from the detector to the source (i.e. in the opposite direction) through the scattering medium [15-17] that acts as a set of polygonal objects. The goal of this simulation is to obtain an interference pattern on the detector surface (Figs 7 and 8). This pattern is formed by a set of points, which are selected randomly on the surface of the detector with normal probability distribution. At each this point, the intensity of light is determined as a result of interference of all rays that intersect in it and reach the surface of the source. The direction of each ray is randomly chosen on the surface of the unit sphere. Beam moving in the environment interacts with the objects placed in it. After collision with an object, we have two types of new rays – the reflected ray and refracted one. The number of necessary rays is largely determined by the geometrical configuration of the system as well as the absorption and scattering coefficients of environment and objects in it. The redistribution of energy between the reflected and refracted rays is calculated using the Fresnel formulas:

$$R_s = \left(\frac{n_1 \cos(\theta_i) - n_2 \cos(\theta_t)}{n_1 \cos(\theta_i) + n_2 \cos(\theta_t)} \right)^2,$$

$$R_p = \left(\frac{n_1 \cos(\theta_t) - n_2 \cos(\theta_i)}{n_1 \cos(\theta_t) + n_2 \cos(\theta_i)} \right)^2,$$

$$T_s = 1 - R_s,$$

$$T_p = 1 - R_p. \qquad (21)$$

Here, R and T are the reflection and transmission coefficients, respectively.

The energy changes associated with each photon beam also occur because of environment absorption around the objects and inside them. We discard the rays, contribution of which to the interference pattern at the detector surface is negligibly small and the rays that do not reach the source. For each beam that has passed from the detector to the source, the optical path is calculated. This is needed to calculate the phase during interference summation of all the rays.

The advantage of this method is the possibility of modeling environments that contain objects of arbitrary topology and the possibility of free positioning the plane detector in space. Another feature of this design is that the accuracy of the interference pattern is governed by the number of rays that are traced from each point on the detector and the density of registration dots.

Disadvantages include the fact that the size of the objects should greatly exceed the wavelength (at least by an order of magnitude) and the considerable time is required for ray tracing.

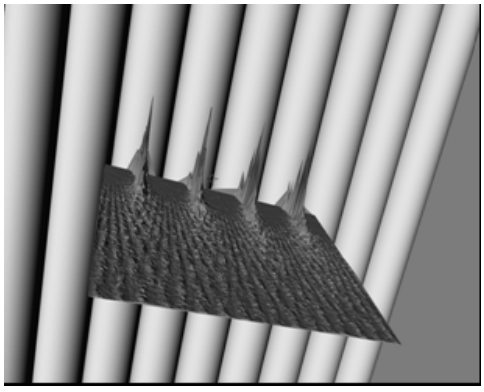

Fig. 7. The interference pattern (radiation passing through a series of cylindrical objects).

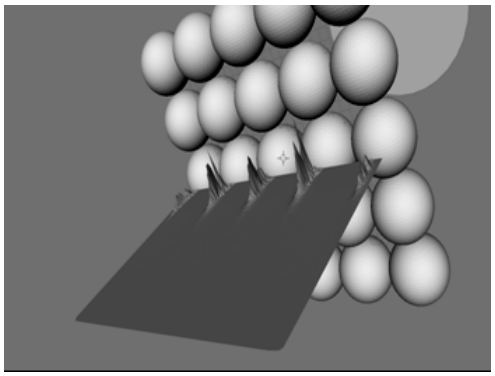

Fig. 8. The interference pattern (radiation passing through a matrix of spherical objects).

The time required for simulation can be reduced by distributing calculations on multiple data centers, which can be done because the algorithm allows parallel computations.

5. Conclusions

Thus, we have implemented two statistical modeling techniques for radiation propagation in epithelial tissue. The modeling results are in good agreement with experimental data. But both models have some limitations. Monte Carlo simulation is based on the Mie theory for spherical particles and doesn't handle scattering particles of arbitrary geometry, which are commonly found inside cells (even cell nuclei often have elliptical form). The ray tracing method works for scattering particles of arbitrary form, but their size must be significantly greater than radiation wavelength, and, since tracing is based on the Fresnel equations, this model doesn't take into account such phenomena as dispersion at all.

Acknowledgements

This work was supported by grants F53/103-2013 from the Fundamental Researches State Fund of Ukraine.

References

1. J.C. Ramella-Roman, S.A. Prahl, S.L. Jacques, Three Monte Carlo programs of polarized light transport into scattering media: part I // *Opt. Express*, **13**(12), p. 4420-4438 (2005).
2. J.C. Ramella-Roman, S.A. Prahl, S.L. Jacques, Three Monte Carlo programs of polarized light transport into scattering media: part I // *Opt. Express*, **13**(25), p. 10392-10405 (2005).
3. *Handbook of Coherent-Domain Optical Methods. Biomedical Diagnostics, Environmental and Material Science*. Eds. V. Tuchin. Kluwer Academic Publishers, 2004.
4. H.W. Jensen, J. Arvo, M. Fajardo, P. Hanrahan, D. Mitchell, M. Pharr, P. Shirley, State of the art in Monte Carlo ray tracing for realistic image synthesis // *SIGGRAPH 2001*, Los Angeles, 2001.
5. X. Wang, L. Wang, V. Lihong, Propagation of polarized light in birefringent turbid media: A Monte Carlo study // *J. Biomed. Opt.* **7**(3), p. 279-290 (2002).
6. O.V. Angelsky, S.B. Yermolenko, O.G. Prydij, A.G. Ushenko, Ye.G. Ushenko, Polarization-interference structure of speckle fields of the rough skin surface // *J. Holography Speckle*, **3**, p. 27-34 (2006).
7. O.V. Angelsky, S.B. Yermolenko, C.Yu. Zenkova, and A.O. Angelskaya, Polarization manifestations of correlation (intrinsic coherence) of optical fields // *Appl. Opt.* **47**, p. 5492-5499 (2008).
8. S. Bartel, A.H. Hielscher, Monte Carlo simulations of the diffuse backscattering Mueller matrix for highly scattering media // *Appl. Opt*. **39**, p. 1580-1588 (2000).
9. L. Wang, S.L. Jacques, L. Zheng, MCML – Monte Carlo modeling of light transport in multi-layered tissues // *Comput. Methods Programs Biomed.* **47**, p. 131-146 (1995).
10. M.J. Rakovic, G.W. Kattawar, M. Mehrubeoglu, B.D. Cameron, L.V. Wang, S. Rastegar, G.L. Cote, Light backscattering polarization patterns from turbid media: Theory and experiment // *Appl. Opt.* **38**, p. 3399-3408 (1999).
11. M. Xu, Electric field Monte Carlo simulation of polarized light propagation in turbid media // *Opt. Exp*. **26**, p. 6530-6539 (2004).
12. S.B. Yermolenko, A.G. Prydij, K.V. Vladychenko, Polarimetry of multi-layer biological tissue // *Proc. SPIE*, **7008**, p. 70082D-1 - 70082D-7 (2008).
13. S.B. Yermolenko, P.V. Ivashko, A.G. Prydiy, I. Gruia, Statistical analysis of polarized images of biotissues for diagnose of their pathological changes // *Optoelectron. Adv. Mater.* – Rapid Communs. **4**(4), p. 527-530 (2010).
14. O.V. Angelsky, S.B. Yermolenko, O.G. Prydij, A.G. Ushenko, Ye.G. Ushenko, Polarization-interference structure of speckle fields of the rough skin surface // *J. Holography Speckle*, **3**, p. 27-34 (2006).
15. O.V. Angelsky, S.B. Yermolenko, C.Yu. Zenkova, A.O. Angelskaya, Polarization manifestations of correlation (intrinsic coherence) of optical fields // *Appl. Opt.* **47**, p. 5492-5499 (2008).
16. I. Gruia, S.B. Yermolenko, M.I. Gruia, P.V. Ivashko, T. Stefanescu, Spectral and biochemical methods for identification of cellular and tissues malignant changes // *Optoelectron. Adv. Mater.* – Rapid Communs. **4**(4), p. 523-526 (2010).
17. A.O. Angelskaya, I. Gruia, S.B. Yermolenko, P.V. Ivashko, M.I. Gruia, Manifestations of linear dichroism changes in cancer biotissues // *Romanian Repts. Phys.* **65**(3), p. 1052-1062 (2013).